Submitted to and accepted by
Surface and Coatings Technology
to appear in early 2011

Chemistry, phase formation, and catalytic activity of thin palladium-containing oxide films synthesized by plasma-assisted physical vapor deposition

D. Horwat[1]*, D. I. Zakharov[1], J.L. Endrino[2], F. Soldera[3], A. Anders[4], S. Migot[1], R. Karoum[1,5], Ph. Vernoux[5], J.F. Pierson[1].

[1] Institut Jean Lamour, Département CP2S, UMR 7198 CNRS-Nancy-Université-UPV-Metz, Ecole des Mines de Nancy, Parc de Saurupt, CS14234, 54042 Nancy, France
[2] Instituto de Ciencia de Materiales de Madrid, C.S.I.C., Madrid 28049, Spain
[3] Department of Materials Science, Saarland University, Campus D3.3, D-66123, Saarbrücken, Germany
[4] Plasma Applications Group, Lawrence Berkeley National Laboratory, 1 Cyclotron Road, Berkeley, CA 94720, USA
[5] Université Lyon 1, CNRS, UMR 5256, IRCELYON, Institut de recherches sur la catalyse et l'environnement de Lyon, 2 avenue Albert Einstein, F-69626 Villeurbanne, France

* Author to whom correspondence should be addressed. Electronic mail: david.horwat@ijl.nancy-universite.fr

Final Version: November 26, 2010

ACKNOWLEDGMENT
The authors acknowledge A. Boreave for help with the catalytic measurements. DIZ acknowledges the European Commission for granting him with the Erasmus Mundus scholarship to perform researches in the framework of the AMASE research master. JL is grateful to the Spanish Ministry of Science and Innovation (projects FIS2009-12964-C05-04 and CSD2008-00023). FS thanks the EFRE Fonds of the European Commission for support of activities within the AME-Lab project. AA acknowledges support by the U.S. Department of Energy under Contract No. DE-AC02-05CH11231.

Chemistry, phase formation, and catalytic activity of thin palladium-containing oxide films synthesized by plasma-assisted physical vapor deposition

D. Horwat[1]*, D. I. Zakharov[1], J.L. Endrino[2], F. Soldera[3], A. Anders[4], S. Migot[1], R. Karoum[1,5], Ph. Vernoux[5], J.F. Pierson[1].

[1] Institut Jean Lamour, Département CP2S, UMR 7198 CNRS-Nancy-Université-UPV-Metz, Ecole des Mines de Nancy, Parc de Saurupt, CS14234, 54042 Nancy, France
[2] Instituto de Ciencia de Materiales de Madrid, C.S.I.C., Madrid 28049, Spain
[3] Department of Materials Science, Saarland University, Campus D3.3, D-66123, Saarbrücken, Germany
[4] Plasma Applications Group, Lawrence Berkeley National Laboratory, 1 Cyclotron Road, Berkeley, CA 94720, USA
[5] Université Lyon 1, CNRS, UMR 5256, IRCELYON, Institut de recherches sur la catalyse et l'environnement de Lyon, 2 avenue Albert Einstein, F-69626 Villeurbanne, France

* Author to whom correspondence should be addressed. Electronic mail: david.horwat@ijl.nancy-universite.fr

Abstract

The chemistry, microstructure, and catalytic activity of thin films incorporating palladium were studied using scanning and transmission electron microscopies, X-ray diffraction, spectrophotometry, 4-point probe and catalytic tests. The films were synthesized using pulsed filtered cathodic arc and magnetron sputter deposition, i.e. techniques far from thermodynamic equilibrium. Catalytic particles were formed by thermally cycling thin films of the Pd-Pt-O system. The evolution and phase formation in such films as a function of temperature were discussed in terms of the stability of PdO and PtO_2 in air. The catalytic efficiency was found to be strongly affected by the chemical composition, with oxidized palladium definitely playing a major role in the combustion of methane. Reactive sputter deposition of thin films in the Pd-Zr-Y-O system allowed us forming microstructures ranging from nanocrystalline zirconia to palladium nanoparticles embedded in a $(Zr,Y)_4Pd_2O$ matrix. The sequence of phase formation is put in relation to simple thermodynamic considerations.

Keywords: Noble metal oxides; Palladium; Thin films; Catalysts; Zr_4Pd_2O; Physical vapor deposition

1. Introduction

Palladium is a transition metal of the platinum group. Even though its d-valence states are not full, palladium resists to oxidation in ambient air. From the point of view of thermodynamics, the palladium oxide PdO is stable below about 800°C in air. Palladium oxidizes only during cooling from high temperatures from approximately 800°C. This thermodynamic behavior suggests to employ plasma-assisted, non-equilibrium techniques of synthesis. Due to the very high cooling rates resulting from the condensation of vapor, physical vapor deposition (PVD) methods have been shown to enable the synthesis of non-equilibrium phases. For instance, gold oxide AuO_x films [1] or highly supersaturated metallic solid solutions [2] can be produced. Therefore, PVD methods are of interest to synthesize palladium-based oxides. To date most studies on thin films incorporating palladium concern metallic Pd (see for instance [3, 4]). Nevertheless some reports rely on the deposition and properties of Pd-based oxide thin films [5-11].

Palladium-based catalysts have been shown to belong to the most effective catalysts for methane combustion [12–19]. While bulk PdO is claimed to be inactive, a thin layer of PdO on metallic Pd is proposed to be the active configuration [19-21]. The predominance of either metallic palladium-supported PdO or a Pd/PdO_y mixture is still highly controversial for catalyst-activated oxidation of methane. In addition to interesting catalytic properties palladium exhibits a very high affinity towards hydrogen and it is able to absorb a very large amount of hydrogen [22]. A Zr-Pd alloy containing oxygen, Zr_4Pd_2O, has been discovered to enable the storage of large amounts of deuterium (hydrogen) [23, 24]. Thus, it can be considered as a key technological material. The compound is only stable at high temperatures and its synthesis required arc melting to reach equilibrium conditions.

In the present paper we investigate the thermal evolution of Pd-Pt-O thin films made far from thermodynamic equilibrium by filtered cathodic arc deposition. We also report on the phase formation in thin films of the Pd-Zr-Y-O system deposited by reactive magnetron co-sputtering. The obtained microstructures are discussed in relation to simple thermodynamic considerations.

2. Materials and methods

2.1. The Pd-Pt-O system

Metallic Pd, Pd oxide and $Pd_{1-x}Pt_x$ oxide films were prepared on yttira stabilized zirconia (YSZ) disk pellets (14 mm in diameter, 1 mm thick) by pulsed filtered cathodic arc deposition [25]. The film composition was measured by secondary neutral mass spectrometry (SNMS) with an 8 keV Ar^+ primary beam; further details of the procedure are given in [8]. The structural characteristics of the films were probed by grazing incidence X-ray diffraction (XRD) using the Co-Kα radiation (0.178897 nm), and the morphology was observed by scanning electron microscopy (SEM, XL30S FEG Philips). Catalytic measurements were performed at atmospheric pressure in a specific quartz reactor. The reactive mixture (RM) contains 5000 ppm CH_4 and 4% O_2 in He. The overall gas flow rate was kept constant at 72 mL min^{-1} (±2 mL min^{-1}). To study catalytic performance (conversion of methane into CO_2) and thermal ageing of the films, three thermal cycles were performed between 250°C and 800°C with a ramp of 10°C min^{-1} and a plateau of 2 h at 800°C for each sample. Further details on the synthesis and analyses procedures can be found in [8]. In addition, high resolution transmission electron microscopy (HRTEM) was performed with a JEOL JEM-2100F microscope to observe the microstructure after the catalytic test. Samples for HRTEM observation were prepared in a focused ion beam (FIB) / scanning electron microscope (SEM) dual beam system (FEI Strata DB235) by using the “in-situ” lift-out technique. Thinning of the foil was done with an acceleration voltage of 30 kV at the beginning and with 5 kV at the end to minimize any possible preparation artifact.

2.2. The Pd-Zr-Y-O system

Thin films of the Pd-Zr-Y-O system were deposited on soda lime glass slides by reactive magnetron co-sputtering of Pd and $Zr_{0.84}Y_{0.16}$ targets (50 mm in diameter, 3 mm thick, with purity higher than 99.9 %). The depositions were done in a 30-L sputtering chamber pumped down via a mechanical pump and a diffusion oil pump leading to a base vacuum of 10^{-4} Pa. The system was equipped with two unbalanced magnetrons separated by 100 mm from each other symmetrically relatively to the axis of the rotating substrate holder. The distances between the glass substrates and the Pd and $Zr_{0.84}Y_{0.16}$ target were fixed to 100 mm and to 50 mm, respectively.

Before deposition the substrates were cleaned by Ar ion impingement using a 100 W radiofrequency glow discharge at 0.3 Pa for 5 minutes on the 20 cm diameter substrate holder. The $Zr_{0.84}Y_{0.16}$ target was powered by an Advanced Energy Pinnacle+ 5 kW DC-pulsed generator. The discharge frequency was fixed at 50 kHz and the reverse time was 4 µs. The current to the target was kept at an average current of 0.7 A. The Pd target was powered by an Advanced Energy MDX 1.5 kW DC generator and the current was varied in the 0 – 0.15 A range.

The chemical composition of the films was determined using an energy-dispersive spectrometer (EDS) coupled with a scanning electron microscope (Philips XL30S FEG). Given the uncertainty of the oxygen determination by EDS, the Pd/(Pd+Zr+Y) atomic ratio was used. The film thickness was measured using the step method with a Talisurf profilometer, allowing an accuracy of ± 20 nm. The electrical conductivity at room temperature was determined using the four-point probe method via a Keithley 2700 multimeter and a Keithley 237 current source. The linear optical absorption coefficient α was determined using the following expression [26]:

$$\alpha = \frac{1}{d} \ln \frac{(1-R)^2}{T} \qquad (1)$$

where d (cm) is the film thickness, and T and R are the optical film transmittance and reflectance, respectively, measured with a Varian Cary 5000 UV-Vis-NIR spectrophotometer. The film structure was probed by X-ray diffraction in θ/2θ mode using Cu-K_α radiation (0.15406 nm) on a Siemens D500 diffractometer. Additionally, transmission electron microscopy (CM 200 Philips) was used to provide further details on the structure and microstructure of selected films.

3. Results

3.1. Thermal decomposition of catalytic films in the Pd-Pt-O system

Some of the characteristics of the films synthesized from sequentially pulsing Pd and Pt cathodes in argon or oxygen are summarized in Table 1. Depending on the conditions, pure palladium, oxidized palladium with a stoichiometry very close to that of PdO and $Pd_{1-x}Pt_xO_y$ ternary oxide with $x = 0.4$ and $x = 0.6$ were produced. The XRD analysis in the as-deposited state (not shown here) showed that pure palladium exhibited the fcc crystalline structure of palladium with an average crystal size of 10 nm as determined by the Scherrer formula [27]. In contrast, the binary and ternary noble metal oxides were found to be “XRD amorphous”. The films were dense with a thickness close to 40 nm for all conditions.

Apart from the heating and cooling periods, all the samples were placed for 6 hours in the CH_4/O_2 mixture used for the catalytic tests. The SEM micrographs of the surfaces of initial Pd, PdO_y and $Pd_{1-x}Pt_xO_y$ thin films are shown in figures 1.a, b and c, respectively. In all cases the surface of the YSZ substrate became observable as the films shrank and transformed into particles of various morphologies. The transformation of the metallic palladium film led to jagged clusters of particles. Most of these clusters are in the 500 nm to 1 µm range. The constituting particles are about 100 nm in size. PdO_y evolved mostly into isolated and rather acute particles. In contrast the ternary oxides transformed into isolated spherically shaped particles exhibiting a smooth surface. The HRTEM pictures corresponding to the observation of selected particles derived from initial Pd, PdO_y and $Pd_{1-x}Pt_xO_y$ conditions are shown in figures 1.d, 1.e and 1.f, respectively. All the samples are crystallized. The microstructure is sensitive to the initial composition. For initial Pd and PdO_y films, different domains are observed inside a particle. Most of the volume consists of nanodomains as shown in figures 1.d and 1.e but some regions exhibit large coherent domains (not shown here). The nanodomains have been identified by Fourier transform to correspond to either Pd or PdO for both initial compositions. In contrast, the thermal treatment of Pt-containing films generated particles almost free of defects and boundaries, i.e. each particle is almost a monocrystalline Pd-Pt alloy as evidenced from the Fourier transform. Therefore, even though it is very difficult to quantify, the crystallization mechanism is very different whether the films contain Pt or not.

X-ray diffractograms revealing the final structure of the samples are displayed in Figure 2. It is observed that the initial chemical composition has a strong impact on the final crystalline state. While crystalline palladium oxide was detected for initially pure and oxidized palladium, Pt-containing films are constituted of crystalline metal. For initially pure palladium, the crystalline signature corresponds to a mixture of metallic Pd and the palladium oxide phase PdO. These observations are in line with optical observations. Effectively, as all the coatings showed a grey color in the as-deposited state, the reddish color characteristic of crystalline PdO appeared after the catalytic tests for the initial PdO_y film and to a lower extent for the initial Pd film. In contrast, the Pt-containing films retained their grey color after the tests.

The third heating cycle of methane conversion during the catalytic test is presented in figure 3.a for the different samples. CO_2 was the only oxidation product of the reaction which can be simply described as:

$$CH_4 + 2\,O_2 \Rightarrow CO_2 + 2\,H_2O \qquad (2)$$

At the first sight it is observed that Pt-containing catalysts show lower conversion efficiency than oxidized and metallic palladium. This is in accordance with the detrimental effect of Pt incorporation into $Pd_{1-x}Pt_x$ for $x \geq 0.33$ reported by Persson et al. for the same reaction [28]. For the highest Pt content ($x = 0.6$) the catalytic conversion is very low and reached only a few percent at 770°C. While the Pt content is decreased to $x = 0.4$, the activity gets higher but only below 680°C, a temperature from which the conversion of methane drops to about 3 percent. Initial Pd and PdO_y films resulted in maximal methane conversions of 54 and 63 percent at 735 and 725°C, respectively. At higher temperatures the activity dropped very fast to become equivalent to that of Pt-containing films at 770°C. The decrease in conversion efficiency at high temperature contains information on the evolution of the chemical composition of the Pd-based catalysts. This feature can be put in relation to the thermal decomposition of the palladium oxide PdO into Pd and oxygen in the 700-750°C temperature range depending on the gas composition and the nature of the support [3, 18, 29].

Figure 3.b. represents the catalytic activity of the samples free of Pt during cycling. If the palladium loading is taken into account, the activity is higher for initial PdO_y than for metallic Pd. Since the size of the particles derived from these films are different, and due to clustering of particles from the initial Pd film, it is difficult to isolate the influences of chemistry and morphology on the catalytic activities. Nevertheless it is interesting to note that the initially oxidized sample exhibited already a high activity at the first heating while the initially metallic film showed a very low activity but then slowly rose as the temperature was increased up to 735°C. Cooling down the two samples from 800°C, a temperature at which surface decomposition should be complete, surface re-oxidation occurs. Thereby, the conversion of hydrocarbons restarts. However, the re-oxidation of the surface occurs at a lower temperature than the decomposition upon heating. Therefore, both materials exhibit an activity hysteresis of about 100°C. Moreover, the conversion efficiency by PdO_y-derived particles is about three times higher than that of Pd-derived particles. This roughly scales with the estimated ratio of Pd atoms available at the surface of the particles or clusters to the total number of Pd atoms, of 16 and 6 percent, respectively.

3.2. Composition-controlled microstructure in the Pd-Zr-Y-O system.

The principal features of the deposited films are summarized in Table 2. By varying the current applied to the palladium target it was possible to progressively change the chemical composition in the synthesized films, characterized by the Pd / (Pd+Zr+Y) atomic ratio. The ratio of Zr to Y is very close to that of the $Zr_{0.84}Y_{0.16}$ target. The oxygen gas flow rate necessary to synthesize transparent YSZ layer by operating the $Zr_{0.84}Y_{0.16}$ target alone was found to be close to 1.5 sccm by keeping all conditions similar to those used for this study. The oxygen content of the gas mixture (at a flow of 6.3 sccm O_2) was therefore enough to ensure that both zirconium and yttrium atoms got oxidized.

The compound formed without incorporation of palladium exhibits the XRD signature of cubic nanocrystalline YSZ (Figure 4). The grain size estimated using the Scherrer formula is 16 ± 2 nm. The incorporation of palladium at a value of Pd / (Pd+Zr+Y) of 0.18 induces a reduction of the intensity of the (111), (220), (311) and (222) diffraction lines accompanied by the disappearance of the (200) and (400) diffraction lines. The disappearance of those diffraction lines can be explained by a change in the crystal shape. No change of grain size could be detected through the use of the Scherrer formula. In addition to the signature of this crystalline phase, a broad feature is observed centered around 37°. Increasing the composition up to Pd / (Pd+Zr+Y) = 0.6, the XRD diffractograms reveal the presence of an amorphous or very fine-grained nanocrystalline phase since only the broad feature is retained. For the highest Pd content, i.e. for Pd / (Pd+Zr+Y) = 0.61, new broad diffraction lines are observed which can be assigned to the (111) and (220) lattice planes of metallic palladium with an average grain size of 3 nm. The diffraction analysis was reproduced after annealing the samples for 2 hours at 300°C in air (not shown) but did not evidenced any obvious structural change.

Spectrophotometry can be very useful to detect in a much more sensitive way than XRD the presence and formation of metallic nanoparticles in a dielectric medium through the surface plasmon resonance (SPR) effect. This effect results in a specific optical absorption usually in the visible part of the spectrum. The film of highest Pd content was too absorbent to give relevant information through this method but the XRD analysis already showed the formation of Pd nanoparticles. The optical absorption curve of as-deposited YSZ shows that the compound is transparent over the visible region. The progressive incorporation of Pd into the coatings produces an increase in the absorption coefficient of the as-deposited films (Figure 5.a) but the typical absorption band related to SPR could only be detected at a chemical ratio Pd/(Pd+Zr+Y) of 0.60. This goes along with the occurrence of a detectable electronic conductivity (see Table 2). These observations are strong clues for the segregation of metallic Pd even though it was not detected by XRD. After annealing the samples at 300°C in air for 2 hours, the SPR band of the sample with Pd/(Pd+Zr+Y) = 0.60 developed and the SPR phenomenon became detectable (Figure 5.b), though very weak, even for the film of the lowest Pd content. Nevertheless, for Pd content below Pd/(Pd+Zr+Y) = 0.60, the conductivity is low and the precipitation of metallic palladium should not be considered as representative for the film microstructure.

Further observations and structural analyses by TEM bring light to the nanometer scale microstructure of the coatings (Figure 6). As a broad XRD feature at low angles has been observed in all the films of the Pd-Zr-Y-O system, it is relevant to try to define its nature. For palladium content in Pd/(Pd+Zr+Y) ranging from 0.18 to 0.61, the main phase of the films was very similar from the structural point of view. It was better defined for Pd/(Pd+Zr+Y) equal to or above 0.31.

The selected area electron diffraction (SAED) characteristic of this phase is presented in figure 6.a. It can undoubtedly be identified as the diffraction pattern of the structure corresponding to Zr_4Pd_2O, a cubic phase (Ti_2Ni-type, $Fd\overline{3}m$) with a very large cell parameter of 1.24 nm that has only been produced so far by arc melting Zr, ZrO_2 and Pd [23, 24]. In figure 6.b, traces of the crystallographic planes can be observed in crystals of typically 5 nm or less. Those traces could be seen even with the conventional TEM used for this study due to the very large cell parameter of the compound. The phase could also be detected as a very fine-grained arrangement (at the limit of the glass state) constituting the matrix of the sample with Pd/(Pd+Zr+Y) = 0.18. Even though the presence of zirconia is evident from the XRD spectrum of the latter sample, it is easily concluded from a TEM observation at higher magnification (figure 6.c) that zirconia is a minority phase for this composition. At the highest Pd loading the XRD analysis did already indicate the segregation of a significant amount of metallic Pd. Palladium nanoparticles can also be found by observing the sample in TEM (figure 6.d.). This has been confirmed by EDS measurements and electron diffraction analysis of the particles (not shown here for space reason). The particles were embedded in a nanocrystalline matrix of the Zr_4Pd_2O structure. Therefore, depending on the palladium loading, the morphology of the films synthesized in the Pd-Zr-Y-O system was found to be a mixture of zirconia and a nanocrystalline phase of Zr_4Pd_2O, by the latter phase alone, or by a mixture of nanocrystalline palladium and Zr_4Pd_2O. It is not clear for the moment to which extent the chemical composition of this phase is affected by the global palladium content but it appears it can be formed over a wide range of compositions despite the fact that palladium shows a limited affinity towards oxygen in normal conditions.

4. Discussion

Depending on its chemical environment and on the temperature, palladium can be oxidized or metallic. In normal conditions palladium is not oxidized. Its oxidation requests thermal heating in an oxidizing atmosphere. PVD methods, which are non-equilibrium in nature, can be used to force the oxidation of noble metals in thin film form during deposition close to room temperature. In pulsed cathodic arc deposition, a plasma is produced containing positive ions of the metal cathode as well as some gas ions. The metal ions are likely to react with oxygen in the presence of a surface. It was thus possible to fabricate Pd-Pt-based oxides in the as-deposited films (see Table 1).

The thermal evolution of such coatings is nevertheless subject to thermodynamics. The standard Gibbs formation energies of PdO and PtO_2 have been plotted in figure 7.a as a function of the temperature. It is observed that palladium oxide is clearly unstable above 850°C. Nevertheless, the decomposition can start in air as low as approximately 430°C and exhibit an equilibrium constant over $3\cdot10^{-2}$ at approximately 730°C [30]. The decomposition of palladium can be expressed as follows:

$$PdO \Rightarrow Pd + \tfrac{1}{2} O_2 \qquad (3)$$

PtO_2, the most stable platinum oxide, decomposes at a temperature of about 450°C [31] following:

$$PtO_2 \Rightarrow Pt + O_2 \qquad (4)$$

The thermal evolution of the $Pd_{1-x}Pt_xO_y$ coatings and the evolution of their catalytic properties can be understood from these simple considerations. The increase in activity of the initially metallic Pd sample during the first cooling can be understood as the oxidation of the surface in contact with the gas mixture. Then, the catalytic activity remains at a high level over cycling unless the same is heated over the decomposition temperature of the surface which occurs at 725°C, i.e. slightly below what thermodynamics predicts for PdO immersed in air. Cooling down the sample below the decomposition temperature initiates its re-oxidation. This is supported by the fact that for a Pd surface already partially oxidized in the as-deposited state, i.e. for the PdO_y sample, the catalytic activity is already high during the first heating and only slightly evolves between cycles 1 and 2. Based on this hypothesis, the addition of platinum into oxidized Pd should affect the catalytic properties by promoting the decomposition of the ternary oxide due to the easier destruction of the Pt-O bonds. For $x = 0.4$, the temperature of maximal conversion is reduced to about 670°C and the activity becomes even negligible for $x = 0.6$. These observations put in relation to the XRD signature show that platinum helps reducing the oxide phase, which in turn significantly affects the catalytic efficiency. Even though a mixture of Pd and PdO, or only PdO, may be active, it is clear from the present results that the surface has to be at least partially oxidized to be efficient for the combustion of methane.

In contrast to the weak reactivity of palladium atoms, zirconium and yttrium ones show a strong affinity towards oxygen (figure 7.b). Under non-equilibrium conditions such as those in a PVD process, the phase formation results from a complex combination of kinetic and thermodynamic factors. It is very much related to the bonding state of the individual atoms and to their relative affinities. Moreover, in reactive sputtering, oxide thin films condensate from neutral as well as ionized oxygen, which affects the phase formation. As the palladium content increases, the microstructure goes first from nanocrystalline zirconia to a mixture of zirconia and nanocrystalline $(Zr,Y)_4Pd_2O$. In this phase, the Zr-O, Pd-O and Zr-Pd distances are close to 0.231, 0.504 and 0.448 nm, respectively (calculated from [20]). Therefore, the bonding of Pd and oxygen atoms is rather limited and the phase formation is more driven by Zr-Pd bonding and oxidation of zirconium atoms. The role of yttrium in the formation of this phase is hard to determine but there are arguments that it must be substituting some Zr atoms:

- The SAED pattern (figure 6.a) shows that the symmetry of Zr_4Pd_2O is retained,
- Yttrium has an atomic radius of 0.178 nm close from that of zirconium (0.160 nm),
- The affinities of zirconium and yttrium towards oxygen are very similar.

To the best of our knowledge there is no Zr-Pd-O phase diagram available in the literature which could be used as a reference for the present discussion. Zr_2Pd is a stable phase of the Zr-Pd phase diagram but exhibits a different crystal structure (I4/mmm space group) than Zr_4Pd_2O. The predominance of $(Zr,Y)_4Pd_2O$ at Pd/(Zr+Y+Pd) in the 0.18-0.60 range shows that bonding Pd to Zr(Y) in the ternary(quaternary) oxide seems more beneficial from the energy balance than the segregation of ZrO_2 and PdO or ZrO_2 and Pd. The range of composition for which the $(Zr,Y)_4Pd_2O$ phase is dominating the microstructure is surprisingly wide, which suggests a high solubility of palladium in it. The segregation of metallic palladium for the highest palladium content could be explained by a combination of two factors:

- The balance between metal and oxygen atoms is shifted in favor of metal atoms as the current applied to the palladium target is increased. The element having the lowest affinity towards oxygen must be the first to segregate in metallic form. We also observed this effect in the Cu-Ag-O system [32]. It is worth noting that changing the gas composition would also affect this balance and the obtained morphologies.
- The solubility of palladium into the $(Zr,Y)_4Pd_2O$ phase cannot be unlimited.

Conclusions

Pulsed filtered cathodic arc and reactive magnetron deposition methods have been used to synthesize palladium-containing thin films of ternary and quaternary noble metal oxides. Due to the weak affinity of palladium towards oxygen, the formation of oxide or metallic phases is very much dependent on the thermal history and nature of the alloying elements. Starting from dense coatings of various chemical compositions in the Pd-Pt-O system, thermal cycling up to 800°C in an oxidizing atmosphere allowed us to produce catalytic particles dispersed at the surface of yttria stabilized zirconia. The decomposition temperature of such catalysts can be tuned by the platinum content which renders the decomposition easier. The possibility to obtain oxidized palladium in the as-deposited state is beneficial to the study of heterogeneous catalytic conversion of methane. It confirms that metallic palladium alone is not the most efficient catalyst. The presence of zirconium and yttrium allows the formation of very different microstructures. Without palladium, yttria stabilized zirconia was formed. Incorporation of approximately one palladium atom for every five metal atoms into the coatings allowed us to synthesize a composite material mostly made up of a finely grained nanocrystalline $(Zr,Y)_4Pd_2O$ phase in which zirconia crystals are embedded. For Pd/(Zr+Y+Pd) ratios of 0.31 to 0.60 only the quaternary phase was observed by X-ray diffraction and transmission electron microscopy. This phase has only been formed so far by arc melting and can find some applications in deuterium (hydrogen) storage. Spectrophotometry and electrical measurements were enough sensitive to detect metallic palladium at the ratio of 0.60. Precipitation of a significant fraction of palladium is observed by slightly increasing the palladium content.

Acknowledgements

The authors acknowledge A. Boreave for help with the catalytic measurements. DIZ acknowledges the European Commission for granting him with the Erasmus Mundus scholarship to perform researches in the framework of the AMASE research master. JL is grateful to the Spanish Ministry of Science and Innovation (projects FIS2009-12964-C05-04 and CSD2008-00023). FS thanks the EFRE Fonds of the European Commission for support of activities within the AME-Lab project. AA acknowledges support by the U.S. Department of Energy under Contract No. DE-AC02-05CH11231.

References

[1] J.J. Pireaux, M. Liehr, P.A. Thiry, J.P. Delrue, R. Caudano, Surf. Sci. 141 (1984) 221-232.
[2] D. Horwat, M. Dehmas, E. Aubry, J. Zollinger, S. Migot, J.F. Pierson, Intermetallics 17 (2009) 421-426.
[3] V. Roche, R. Karoum, A. Billard, R. Revel, P. Vernoux, J. Appl. Electrochem. 38 (2008) 1111-1119.
[4] P. Brault, A.L. Thomann, C. Andreazza-Vignolle, Surf.Sci. 406 (1998) L597-L602.
[5] V. Cassina, L. Gerosa, A. Podestà, G. Ferrari, M. Sampietro, F. Fiorentini, T. Mazza, C. Lenardi, P. Milani, Phys. Rev. B 79 (2009) 115422.
[6] Y. T. Lee, J. M. Lee, Y. J. Kim, J. H. Joe, W. Lee, Nanotechnology 21 (2010) 165503
[7] Q. Liu, T. Fukaya, J. Nanosci. Nanotechnol. 7 (2007) 362-367.
[8] D. Horwat, J.L. Endrino, A. Boreave, R. Karoum, J.F. Pierson, S. Weber, A. Anders, Ph. Vernoux, Catal. Comm. 10 (2009) 1410-1413.
[9] R. Catrin, D. Horwat, J.F. Pierson, S. Migot, Y. Hu, F. Mücklich, Appl. Surf. Sci., in press, doi:10.1016/j.apsusc.2010.11.060.
[10] M. Kozłowski, R. Diduszko, K. Olszewska, H. Wronka, E. Czerwosz, Vacuum, 82 (2008) 956-961.
[11] Y.T. Lee, J.M. Lee, Y.J. Kim, J.H. Joe, W. Lee, Nanotechnology 21 (2010) 165503.
[12] F. H. Ribeiro, M. Chow, R. A. DallaBetta, J. Catal. 146 (1994) 537-544.
[13] C.A.Müller, M. Maciejewski, R. A. Koeppel, R. Tschan, A. Baiker, J. Phys. Chem. 100 (1996) 20006-20014.
[14] K. Fujimoto, F. H. Ribeiro, M. Avalos-Borja, E. Iglesia, J. Catal. 179 (1998) 431-442.
[15] R. A. DallaBeta, T. Rostrup-Nielsen, Catal. Today 47 (1999) 369-375.
[16] G. Centi, J. Mol. Catal. A 173 (2001) 287-312.
[17] P. Gelin, M. Primet, Appl. Catal. B 39 (2002) 1-37.
[18] R. J. Farrauto, M. C. Hobson, T. Kennelly, E. M. Waterman, Appl. Catal. A 81 (1992) 227-237.
[19] J.N. Carstens, S.C. Su, A.T. Bell, J. Catal. 176 (1998) 136-142.
[20] R. Burch, F. J. Urbano, Appl. Catal. A 124 (1995) 121-138.

[21] S.C. Su, J.N. Carstens, A. T. Bell, J. Catal. 176 (1998) 125-135.
[22] A. Züttel, Mater. Today 6 (2003) 24.
[23] H.W. Brinks, A.J. Maeland, B.C. Hauback, R.C.. Bowman, J.S. Cantrell, J. Alloys Compd. 361 (2003) 108-112.
[24] J.S. Cantrell, R.C. Bowman, A.J. Maeland, J. Alloys Compd. 330-332 (2002) 191-196.
[25] A. Anders, Cathodic Arcs: From Fractal Spots to Energetic Condensation, Springer, New York, 2008.
[26] H.G. Tompkins, E.A. Irene, Handbook of Ellipsometry, William Andrew Publishing, Noyes, 2005.
[27] H.P. Klug, L.E. Alexander, X-Ray Diffraction Procedures for Polycrystalline and Amorphous Materials, Wiley, 1974.
[28] K. Persson, A. Erssona, K. Janssonb, N. Iverlund, S. Järås, J.Catal. 231 (2005) 139-150.
[29] T. Furuya, K. Sasaki, Y. Hanakata, T. Ohhashi, M. Yamada, T. Tsuchiya, Y. Furuse, Catal. Today 26 (1995) 345-350.
[30] O. Knacke, O. Kubaschewski, K. Heselmann, Thermo-Chemical Properties of Inorganic Substances, Springer Verlag, Berlin, 2nd edition, 1991.
[31] Samsonov, Gregorii Valentinovich, The Oxide Handbook, IFI/Plenum, New York,1973
[32] J.F. Pierson, D. Horwat, Appl. Surf. Sci. 253 (2007) 7522-7526.

Table Captions

Table 1: Deposition conditions and characteristics of thin films synthesized by pulsed filtered cathodic arc in the Pd-Pt-O system

Table 2: Deposition conditions and characteristics of thin films synthesized by reactive magnetron co-sputtering in the Pd-Zr-Y-O system

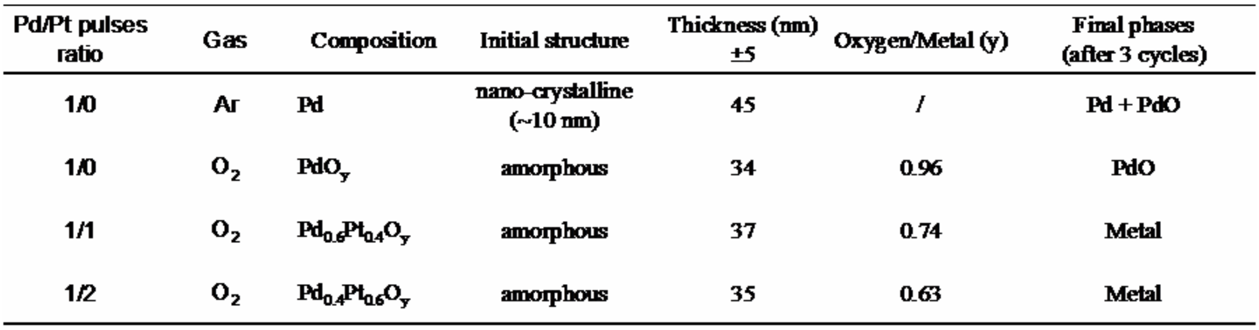

Pd/Pt pulses ratio	Gas	Composition	Initial structure	Thickness (nm) ±5	Oxygen/Metal (y)	Final phases (after 3 cycles)
1/0	Ar	Pd	nano-crystalline (~10 nm)	45	/	Pd + PdO
1/0	O_2	PdO_y	amorphous	34	0.96	PdO
1/1	O_2	$Pd_{0.6}Pt_{0.4}O_y$	amorphous	37	0.74	Metal
1/2	O_2	$Pd_{0.4}Pt_{0.6}O_y$	amorphous	35	0.63	Metal

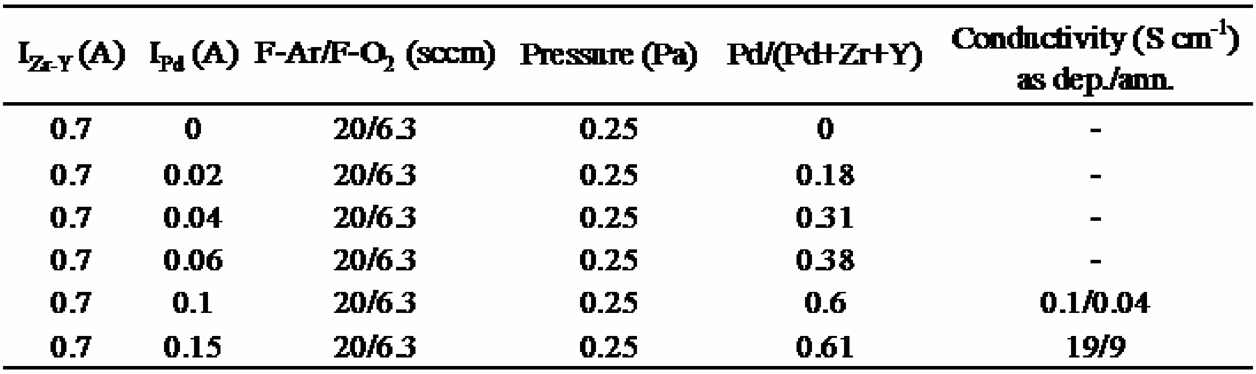

I_{Zr-Y} (A)	I_{Pd} (A)	F-Ar/F-O_2 (sccm)	Pressure (Pa)	Pd/(Pd+Zr+Y)	Conductivity (S cm^{-1}) as dep./ann.
0.7	0	20/6.3	0.25	0	-
0.7	0.02	20/6.3	0.25	0.18	-
0.7	0.04	20/6.3	0.25	0.31	-
0.7	0.06	20/6.3	0.25	0.38	-
0.7	0.1	20/6.3	0.25	0.6	0.1/0.04
0.7	0.15	20/6.3	0.25	0.61	19/9

Figure Captions

Figure 1: SEM/TEM micrographs of the surface of Pd (a)/(d), PdO_Y (b)/(e) and $Pd_{1-x}Pt_xO_Y$ (c)/(f) thin samples prepared by filtered cathodic arc after 6 hours at 800°C in oxidizing atmosphere (5000 ppm CH_4 and 4% O_2).

Figure 2: X-Ray diffractograms of Pd, PdO_y and $Pd_xPt_{1-x}O_y$ films synthesized by filtered cathodic arc after 6 hours at 800°C in oxidizing atmosphere (5000 ppm CH_4 and 4% O_2).

Figure 3: Methane conversion (a) and catalytic activity (b) of Pd, PdO_y and $Pd_xPt_{1-x}O_y$ films synthesized by filtered cathodic during the third heating cycle up to 800°C in oxidizing atmosphere (5000 ppm CH_4 and 4% O_2).

Figure 4: X-ray diffractograms of thin films of the Pd-Zr-Y-O system deposited by reactive magnetron sputtering.

Figure 5: Evolution in the UV-visible range of the optical absorption coefficient of thin films of the Pd-Zr-Y-O system deposited by reactive magnetron sputtering in the as deposited state (a) and after 2 hours annealing in air (b).

Figure 6: SAED pattern (a) and bright field TEM micrograph (b) characteristic of a Zr_4Pd_2O-like phase. Bright field TEM micrograph and SAED pattern of a thin film with a Pd(Pd+Zr+Y) ratio of 0.18 (c). TEM bright field micrograph showing details of a thin film with a Pd(Pd+Zr+Y) ratio of 0.61 (d).

Figure 7: Evolution of (a) the standard Gibbs energy of formation of PdO and PtO_2, and (b) of PdO, ZrO_2 and Y_2O_3, both as a function of temperature. The values are given for 1 mole of metal.

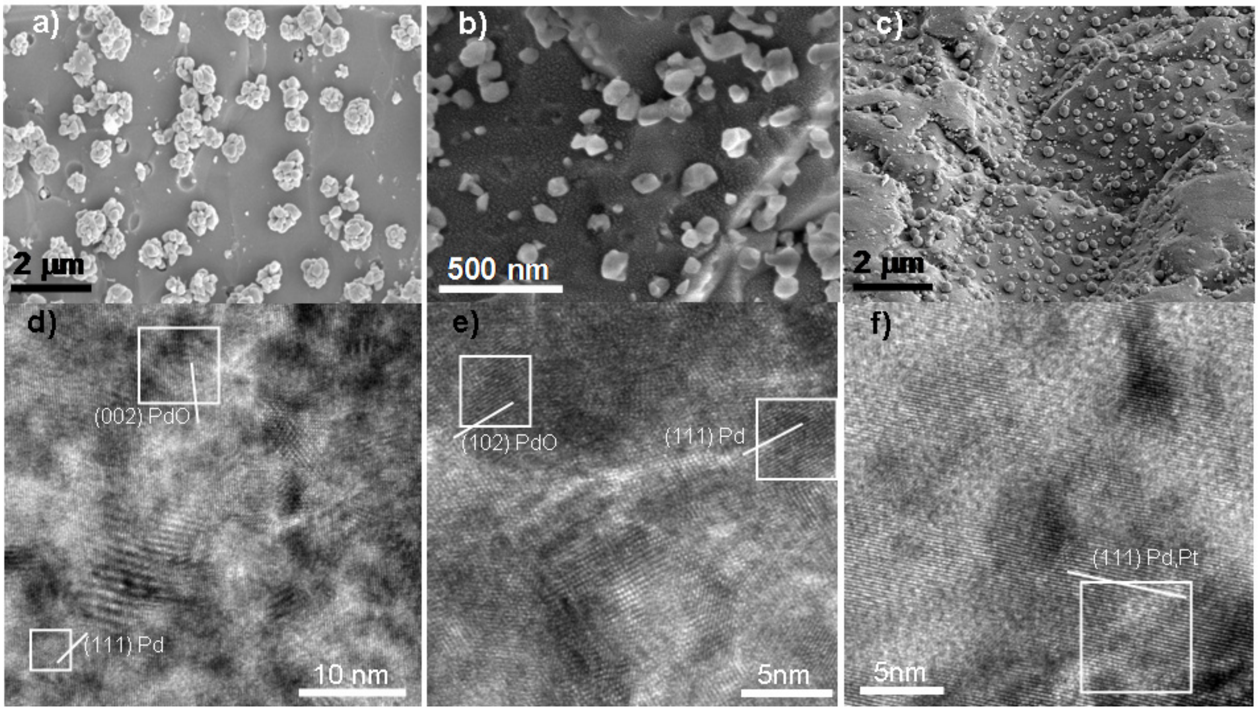
a)
2 µm
b)
500 nm
c)
2 µm
d)
(002) PdO
(111) Pd
10 nm
e)
(102) PdO
(111) Pd
5nm
f)
(111) Pd,Pt
5nm

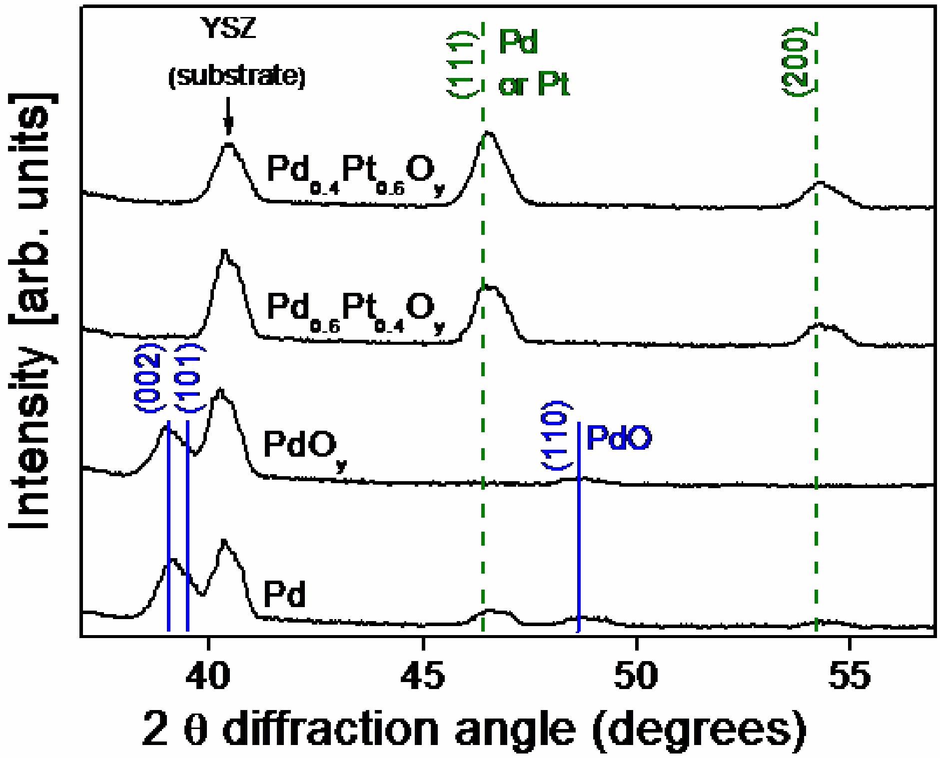
YSZ
(substrate)
(111)
Pd
or Pt
(200)
Pd0.4Pt0.6Oy
Pd0.6Pt0.4Oy
(002)
(101)
PdOy
(110)
PdO
Pd
Intensity [arb. units]
40
45
50
55
2 θ diffraction angle (degrees)

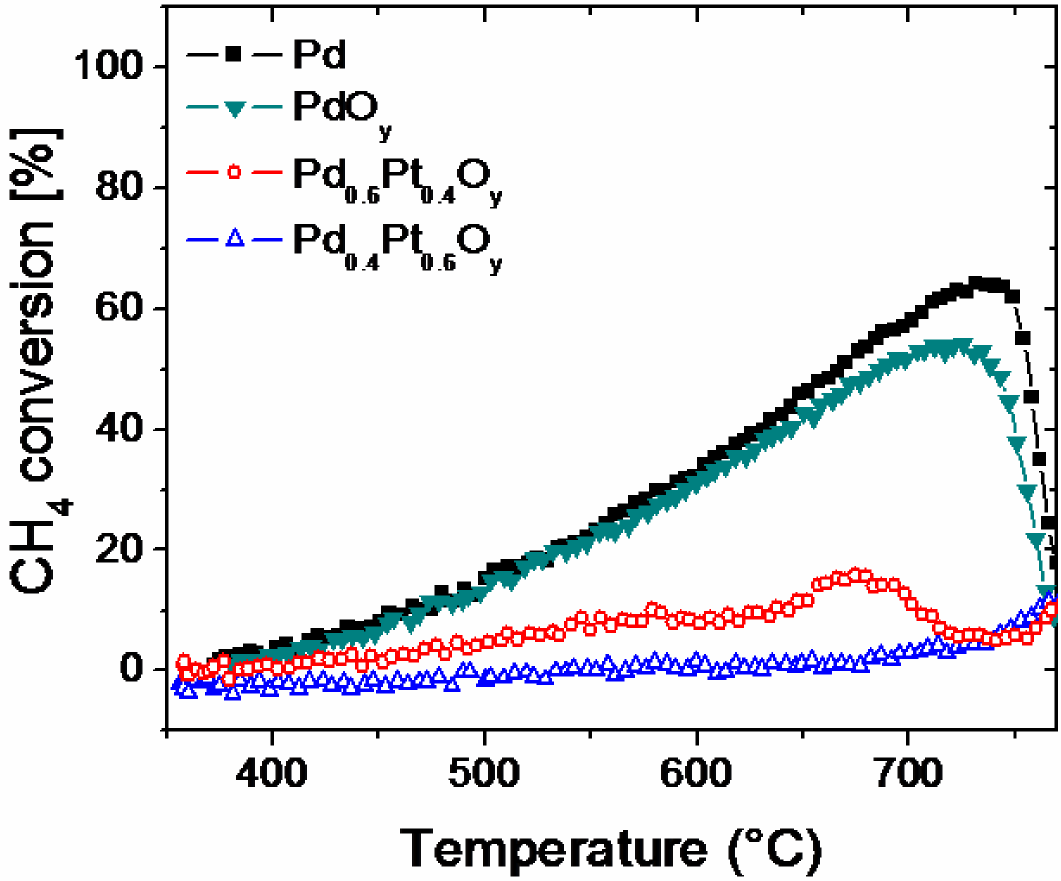
Pd
PdO$_y$
Pd$_{0.6}$Pt$_{0.4}$O$_y$
Pd$_{0.4}$Pt$_{0.6}$O$_y$
CH$_4$ conversion [%]
Temperature (°C)
0
20
40
60
80
100
400
500
600
700

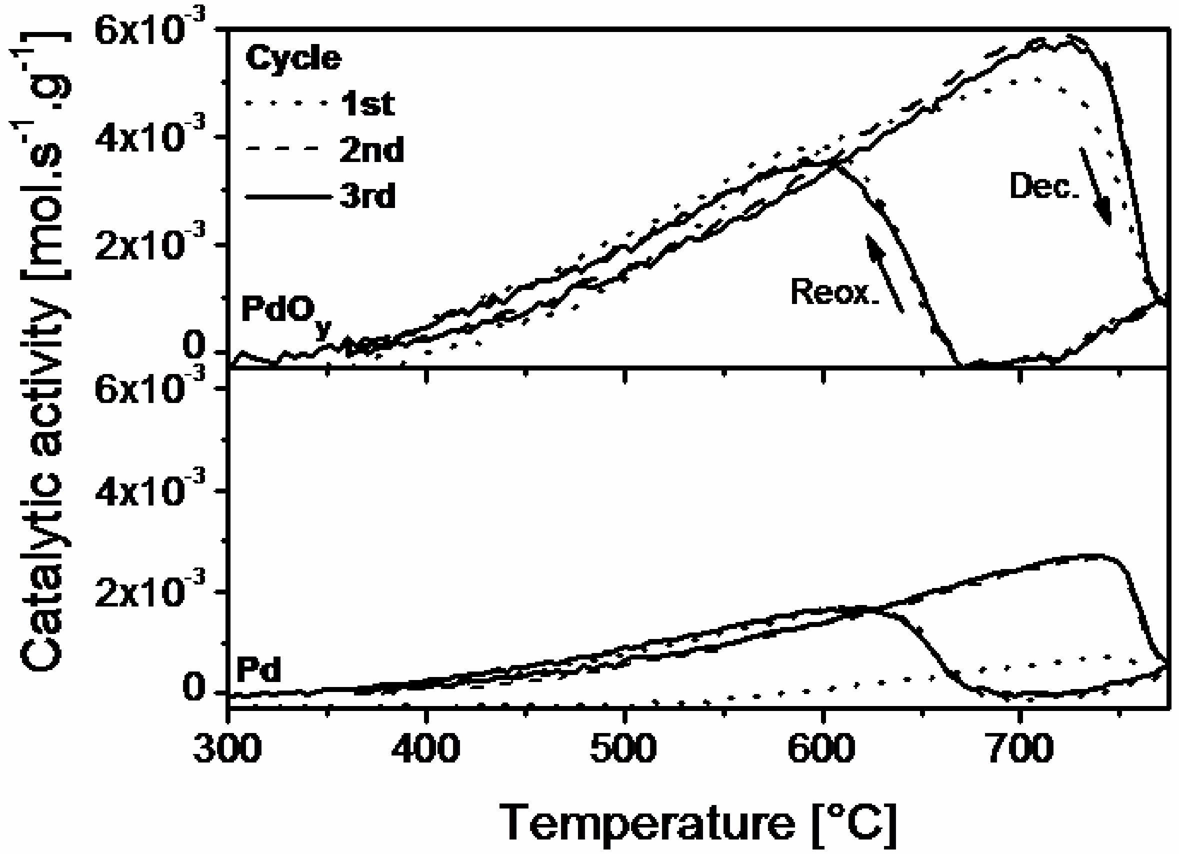
Catalytic activity [mol.s^{-1}.g^{-1}]
6x10^{-3}
4x10^{-3}
2x10^{-3}
0
Cycle
1st
2nd
3rd
PdO$_y$
Reox.
Dec.
Pd
300
400
500
600
700
Temperature [°C]

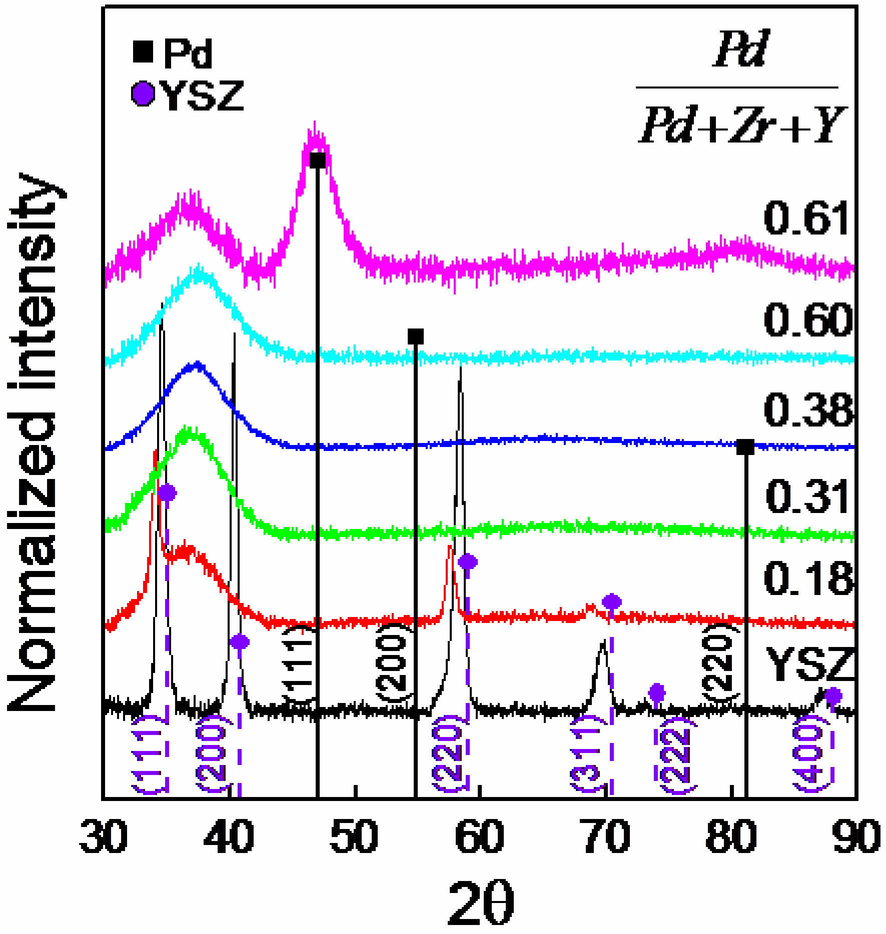
■ Pd
● YSZ
Pd / (Pd+Zr+Y)
0.61
0.60
0.38
0.31
0.18
YSZ
(111)
(200)
(220)
(111)
(200)
(220)
(311)
(222)
(400)
Normalized intensity
30
40
50
60
70
80
90
2θ

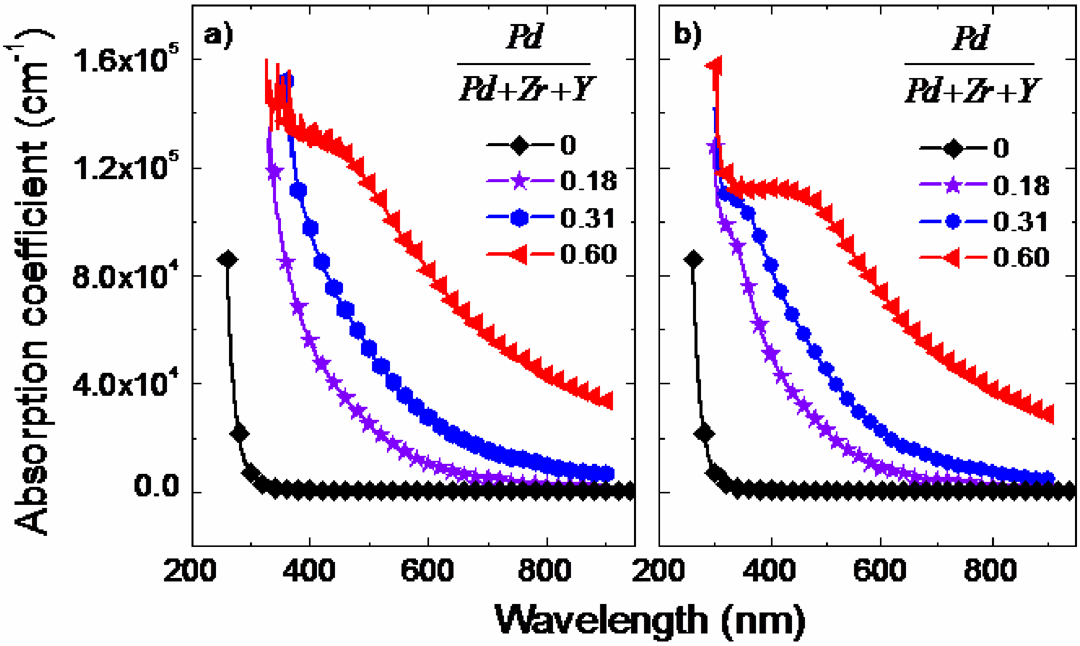
a)
b)
Absorption coefficient (cm^{-1})
1.6x10^5
1.2x10^5
8.0x10^4
4.0x10^4
0.0
200
400
600
800
Wavelength (nm)
$\frac{Pd}{Pd+Zr+Y}$
0
0.18
0.31
0.60

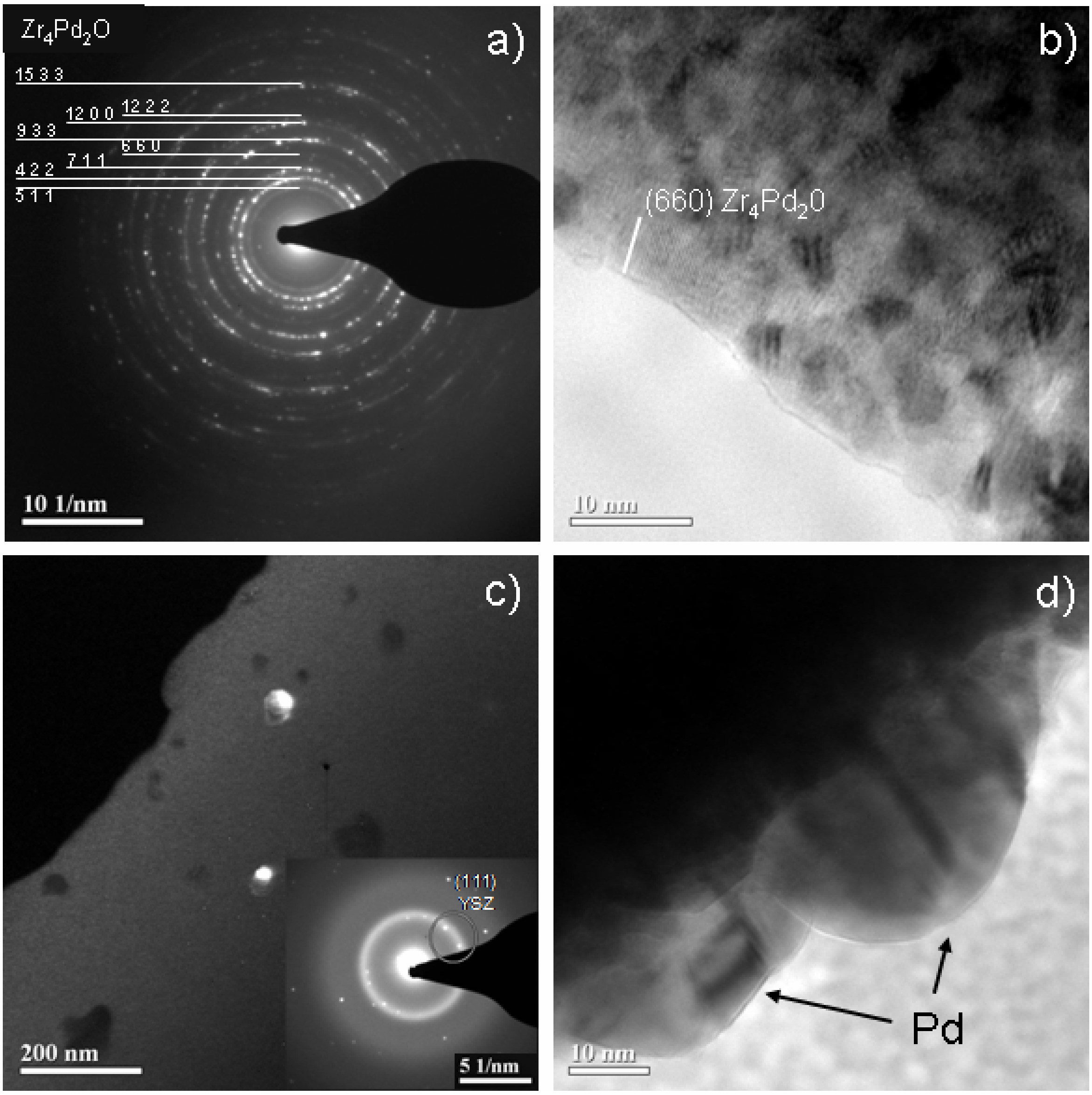
Zr$_4$Pd$_2$O
a)
15 3 3
12 0 0
12 2 2
9 3 3
6 6 0
7 1 1
4 2 2
5 1 1
10 1/nm
b)
(660) Zr$_4$Pd$_2$0
10 nm
c)
(111)
YSZ
200 nm
5 1/nm
d)
Pd
10 nm

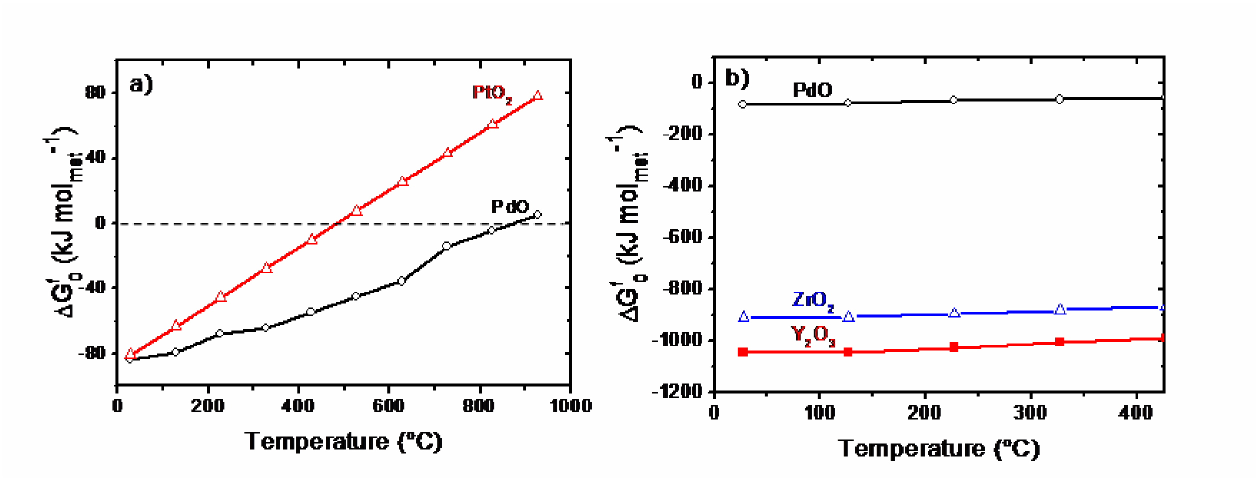
a)
PtO$_2$
PdO
ΔG^f_0 (kJ mol$_{met}^{-1}$)
80
40
0
-40
-80
0
200
400
600
800
1000
Temperature (ºC)
b)
PdO
ZrO$_2$
Y$_2$O$_3$
ΔG^f_0 (kJ mol$_{met}^{-1}$)
0
-200
-400
-600
-800
-1000
-1200
0
100
200
300
400
Temperature (ºC)